Chain Cluster Polymerization and Alkali Metal Intercalation into Niobium Ditelluride

R. Guzmán, J. Morales, and J. L. Tirado*

Departamento de Química Inorgánica e Ingeniería Química, Facultad de Ciencias, Universidad de Córdoba, Avda. San Alberto Magno s/n, 14004 Córdoba, Spain

Received December 8, 1993•

Electrochemical lithium intercalation into 1T-$NbTe_2$ takes place by progressive filling of the distorted octahedral sites in the interlayer space leading to an increase in the c_m parameter. The monoclinic structure and niobium ribbon chain modulation are preserved during lithium intercalation. On the contrary, different modulated structures are observed in the products of sodium intercalation. For $Na_{0.6}NbTe_2$, a $a27^{1/2} \times a27^{1/2}$ superlattice and a basal spacing of 9.89 Å are observed. The geometric relationships between ribbon chain and $3a \times 3a$ modulations in 1T-transition metal dichalcogenides are consistent with a trimerization of $3a3^{1/2} \times a$ modulations due to the changes in the d-band electron count and metal–metal bonding with intercalation. For $NaNbTe_2$, a fully intercalated phase with basal spacing of 8.04 Å and sodium ions in trigonal prismatic coordination is observed. The differences in bond ionicity for Li and Na account for these effects.

Introduction

The structure and reactivity of layered transition-metal chalcogenides have been the subject of extensive research work during the last 2 decades. Some important topics in their study are charge density wave (CDW) phenomena and metal clustering,[1-5] intralayer chalcogen–metal and interlayer chalcogen–chalcogen interactions,[4,6] and structural anomalies by intercalation of electron-donating species in the interlayer space.[7-10]

The group of CdI_2-type compounds 1T-MX_2 (M = transition metal; X = S, Se, Te) with d^0–d^3 M ions in nearly octahedral coordination exhibit a continuously increasing number of structural modifications which are in turn suitable host solids in alkali metal intercalation reactions.[11,12] Metal clustering leads to distortions of the hexagonal lattice found in d^0 1T-TiS_2 into different superstructures which include $a3^{1/2} \times a3^{1/2}$ (1T-MoS_2),[11] $2a \times 2a$ (1T-$TiSe_2$),[4] $a7^{1/2} \times a7^{1/2}$ (1T-VSe_2), $3a \times 3a$ (1T-VSe_2),[1] $a13^{1/2} \times a13^{1/2}$ (1T-TaS_2, 1T-$TaSe_2$),[13] $4a \times 4a$ (1T-VSe_2),[14] and $a19^{1/2} \times a19^{1/2}$ (1T-$NbTe_2$),[15] and zigzag, ribbon, and diamond-chain clustering found 1T-MX_2 with d^2, $d^{4/3}$ and d^3 ions, respectively.[3,4] Most of these structural distortions have recently been examined by using the concepts of hidden 1-D Fermi surface nesting and local chemical bonding, which explain the d-electron count dependence of the structural modulations and the multicenter σ-bonding interactions around metal ions.[4] Accordingly, zigzag chains result from dimerization of metal atoms along, for example, the a and $(a + b)$ directions due to the existence of two half-filled 1-D bands in d^2 ions. Ribbon chains result from trimerizations caused by two one-third filled bands in $d^{4/3}$ ions. Diamond chains are the result of dimerizations along three directions caused by three half-filled 1-D bands. More recently, the $a3^{1/2} \times a3^{1/2}$ superstructure was ascribed to trimerization along a, b, and $(a + b)$ directions when the three 1-D bands are one-third filled in d^2 1T-MoS_2.[5]

On the other hand, the intercalation of electron donor species may affect the d-electron count and thus the level of metal clustering in these solids. The geometric similarities between the electron diffraction patterns of 1T-TaS_2 intercalated with Na, K, and Eu have been considered as an indirect proof that the observed $a3^{1/2} \times a3^{1/2}$ and $3a \times 3a$ superlattices were intrinsic to the TaS_2 lamellae in the intercalated solids.[14] These modulations contrast with the $a13^{1/2} \times a13^{1/2}$ usually found in d^1 1T-TaS_2 and are probably indicative of an increased d-electron count by charge transfer phenomena.

Charge transfer may also result from chalcogen-chalcogen interactions as found in 1T-MTe_2 (M = V, Nb, Ta).[16,17] In these tellurides the presence of interlayer Te-Te interactions increase the Te p-block band energy and favor a d-electron count close to $d^{4/3}$.[6] This band electronic structure leads to a ribbon-chain modulation of the metal ions which is an intermediate situation between the $a13^{1/2} \times a13^{1/2}$ clustering found in d^1 1T-MX_2 systems and the zigzag chains of d^2.[4]

Extra periodicities may also result from regular arrays of intercalated species either between the same undistorted lamellae or by alternating empty interlayers with fully intercalated interlayers (staging phenomena). Electrochemical[18] and X-ray diffraction data[19] suggest that alkali metal ions intercalated into TiS_2 show different three-dimensional ordered superlattices which include $a3^{1/2} \times a3^{1/2}$ superstructure for stage 2 and 3 Na_xTiS_2 phases, $2a \times 2a$ and $2a \times a3^{1/2}$ for stage 1 and 2 Na_xTiS_2 phases, and $a3^{1/2} \times a3^{1/2}$ and $2a \times 2a$ superstructures in Li_xTiS_2 crystals.[19]

The electronic structure and structural distortions of group 5 metal ditellurides offer interesting opportunities for further insight in the above topics. Their structure has been recently reexamined[6] and evidence on the intercalation chemistry of 1T-VTe_2 was recently reported.[20] Here, the effects of alkali metal intercalation in metal clustering of niobium ditelluride are studied.

• Abstract published in *Advance ACS Abstracts*, June 1, 1994.

(1) van Bruggen, C. F.; Haas, C.; Wiegers, G. A. *J. Solid State Chem.* **1979**, *27*, 9.
(2) Kertesz, M.; Hoffmann, R. *J. Am. Chem. Soc.* **1984**, *106*, 3453.
(3) Canadell, E.; LeBeuze, A.; El Khalifa, M. A.; Chevrel, R.; Whangbo, M. H. *J. Am. Chem. Soc.* **1989**, *111*, 3778.
(4) Whangbo, M. H.; Canadell, E. *J. Am. Chem. Soc.* **1992**, 114, 9587.
(5) Rovira, C.; Whangbo, M. H. *Inorg. Chem.* **1993**, *32*, 4049.
(6) Canadell, E.; Jobic, S.; Brec, R.; Rouxel, J.; Whangbo, M. H. *J. Solid State Chem.* **1992**, *99*, 189.
(7) Rouxel, J. *J. Solid State Chem.* **1976**, *17*, 223.
(8) Whittingham, M. S. *Science* **1976**, *192*, 1126.
(9) Murphy, D. W.; Di Salvo, F. J.; Hull, G. W.; Waszczak, J. *Inorg. Chem.* **1976**, *15*, 17.
(10) Murphy, D. W.; Trumbore, F. A. *J. Cryst. Growth* **1977**, *39*, 185.
(11) Wypych, F.; Schöllhorn, R. *J. Chem. Soc., Chem. Commun.* **1992**, 1386.
(12) Wypych, F.; Sollmann, K.; Schöllhorn, R. *Mater. Res. Bull.* **1992**, *27*, 545.
(13) Wilson, J. A.; Di Salvo, F. J.; Mahajan, S. *Adv. Phys.* **1975**, *24*, 117.
(14) Williams, P. M. in *Crystallography and Crystal Chemistry of Materials with Layered Structures*; Lévy, F., Ed.; Reidel: Dordrecht, The Netherlands, 1976; p 70.
(15) van Landuyt, J.; van Tendeloo, G.; Amelinckx, S. *Phys. Status Solidi A* **1974**, *26*, 585.
(16) Brown, B. E. *Acta Crystallogr.* **1966**, *20*, 264.
(17) Bronsema, K. D.; Bus, G. W.; Wiegers, G. A. *J. Solid State Chem.* **1984**, *53*, 415.
(18) Thompson, A. H. *J. Electrochem. Soc.* **1979**, *126*, 608.
(19) Hibma, T. *J. Solid State Chem.* **1980**, *34*, 97.

0020-1669/94/1333-3164$04.50/0

Chain Superposition

A geometrical approach to the relationships between chain and 2-D structural modulations of 1T-MX_2 is carried out here. It has been suggested that the triangular clusters and isolated atoms which are present in a $2a \times 2a$ superstructure can be considered as a superposition of three equivalent chain clusters and are energetically favorable when only nearest neighbors interactions are taken into account.[1] This is graphically described in Figure 1a. Metal atoms involved in opposite metal dimerization effects along $(a, -a)$, $(b, -b)$ and $(a + b, -a - b)$, resulting from the three sets of zigzag chains, remain in udistorted positions. Uncompensated metal dimerization effects origin a displacement of three or each four metal atoms leading to the formation of triangular clusters. The equivalency in the hidden band concept is a trimerization of zigzag chains with two half-filled 1-D bands. This is achieved by three metal atoms each one forming two dimers (i.e. in formal d^2 configuration as in zigzag or $a3^{1/2} \times a3^{1/2}$ modulations) and one fully compensated metal atom with a formal d^6 electron count. The average is a d^3 ion configuration. NbS is characterized by a $2a \times 2a$ modulation.[1] A description of the electronic structure of this compound based in d^3 ions leads to the expected electron count. This is not the case however for 1T-$TiSe_2$, where it was shown that the energy lowering that gives rise to the $2a \times 2a$ structural modulation does not occur in the t_{2g}-block band but in the Se p-block bands.[4]

Similarly, the diamond chain modulation has been ascribed to the dimerization of zigzag chains with two half-filled bands.[3,4] Geometrically, this relationship is also resolved in Figure 1b. Again, each dimerization affecting a metal atom contributes with one electron to its total electron count. As every atom is involved in three dimerizations, the average configuration is still d^3 as confirmed by hidden band nesting considerations (three half-filled 1-D bands).[4] The extent of nearest neighbor interactions conditions the adoption of a $2a \times 2a$ modulation or diamond chain formation by d^2 ions.

The possible formation of the $3a \times 3a$ superstructure by trimerization of ribbon chains differing by 60°, each one with two half filled 1-D bands, is also included in Figure 1. The resulting superstructure contains hexagonal clusters similar to those found in $a7^{1/2} \times a7^{1/2}$ and isolated atoms. The relationships between electron count and the adoption of this trimer is somehow more complex than in the above models due to the presence of trimerizations of metal atoms in ribbon chains and in hexagonal clusters. The expected electron count for the ribbon chains ($d^{4/3}$) is clearly resolved as two sets of trimerizations affect each atom, each one raising the electron count by $^2/_3$. The $3a \times 3a$ superstructure includes two atoms that remain unchanged, as a result of being each one affected by six compensated metal trimerizations and seven atoms affected by a total of three trimerizations. The average electron count per metal atom is then $(2 \times 6 \times {}^2/_3 + 3 \times 2)/9 = 1.56$, a value which is in the 1–2 range. It should be noted that several examples of this superstructure are found in the literature for metal ions having an electron count between 1 and 2.[14,21]

Experimental Section

Powdered samples for monoclinic 1T-$NbTe_2$ were obtained by direct synthesis from the elements at 1000 °C in evacuated silica ampoules. Niobium metal and tellurium were suppied by Strem Chemicals. The electrochemical intercalation of lithium and sodium was studied in A/$ACIO_4$(PC)/telluride test cells (A = Li, Na). The electrochemical cells were prepared inside the drybox by placing a clean metal disk, two glass fiber separators soaked with the electrolyte solution and a pellet of the telluride concerned into a Teflon container with two stainless steel terminals. The cathode pellets (7-mm diameter) were prepared by pressing 12–20 mg of $NbTe_2$ on an inert copper substrate (Merck, 99.7%). Step potential electrochemical spectroscopy was carried out at 25 °C by using a multichanel microprocessor-controlled system, MacPile. An initial relaxation of the cells was allowed until the condition $\Delta V/\Delta t \leq 1$ mV h^{-1} was attained. The spectra were recorded with −10 mV h^{-1} voltage steps. The average alkali metal composition of the cathode material was

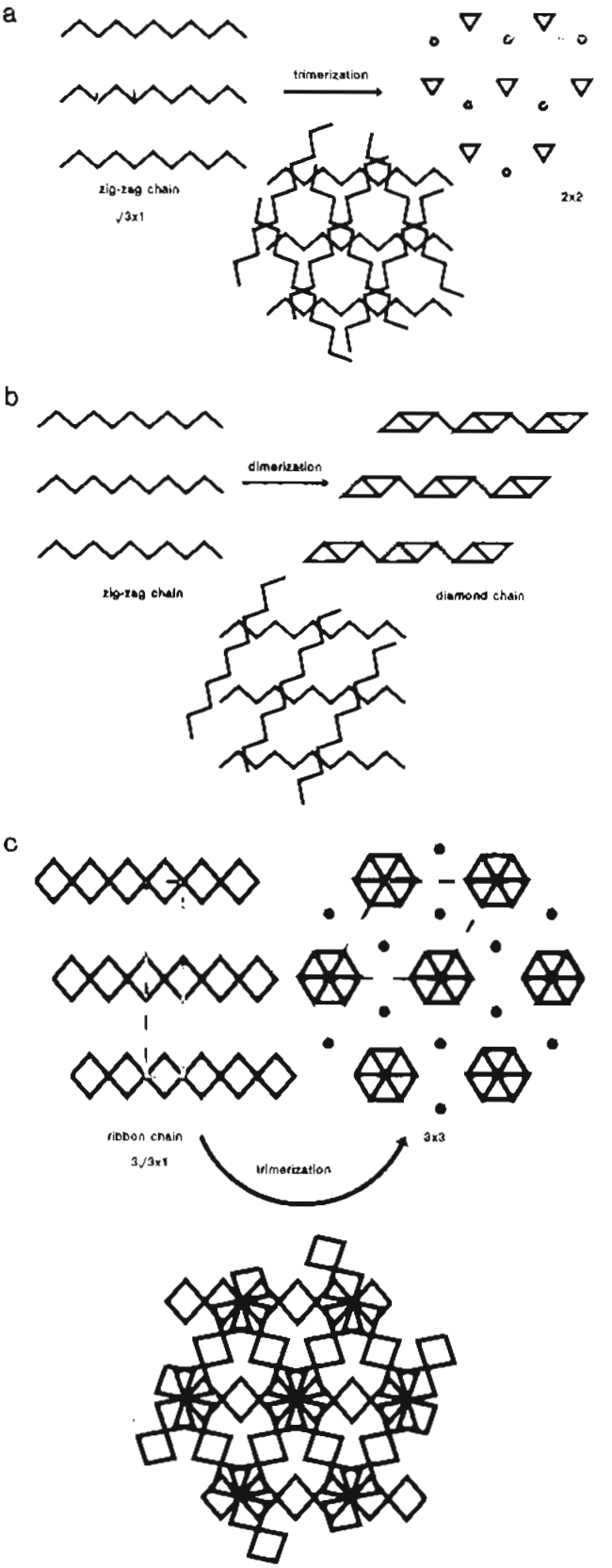

Figure 1. Schematic projection along [001] of (a) intralayer zigzag chain clustering of metal atoms and its trimerization to a $2a \times 2a$ modulation, (b) intralayer zigzag chain clustering of metal atoms and its dimerization to diamond-chain clustering, and (c) intralayer ribbon chain clustering of metal atoms and its trimerization to a 3×3 modulation.

(20) Guzmán, R.; Morales, J.; Tirado, J. L. *J. Mater. Chem.* **1993**, *3*, 1271.
(21) Ritter, C.; Schöllhorn, R. *Solid State Commun* **1987**, *61*, 117.

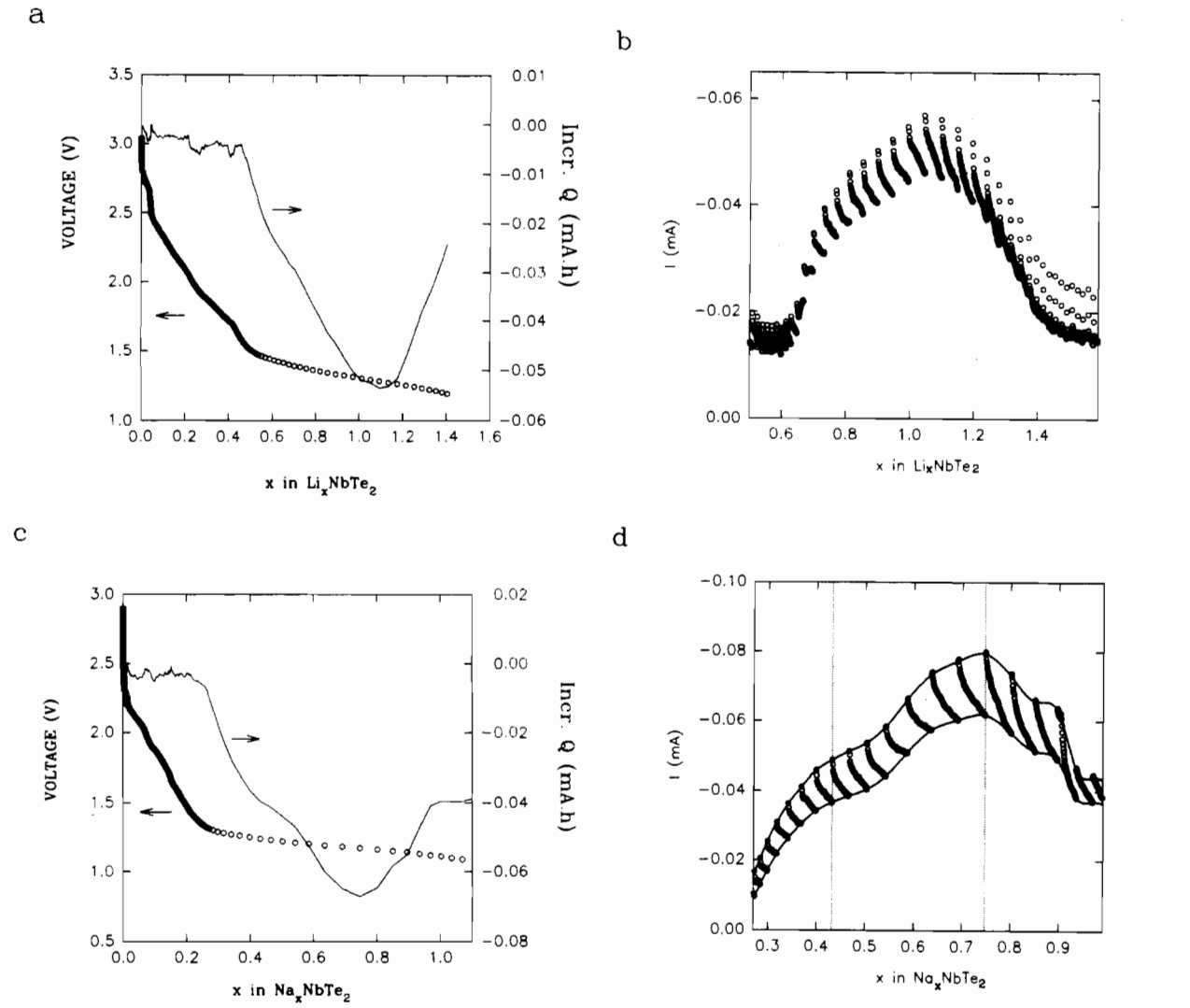

Figure 2. Results of step potential electrochemical spectroscopy: (a) incremental capacity and voltage vs composition of $Li/LiClO_4(PC)/NbTe_2$ cells; (b) current relaxation vs composition of $Li/LiClO_4(PC)/NbTe_2$ cells; (c) incremental capacity and voltage vs composition of $Na/NaClO_4(PC)/NbTe_2$ cells; (d) current relaxation vs composition of $Na/NaClO_4(PC)/NbTe_2$ cells.

calculated from the amount of electron charge transferred to the active material, on the assumption that no current flow was due to side reactions. All spectra were recorded in triplicate to ensure reproducibility. X-ray powder diffractometry (XPD) was carried out using a Siemens D500 diffractometer furnished with Cu Kα radiation and a graphite monochromator. For intercalated phases, a plastic fiber was used to cover the sample in order to avoid undesirable reactions with air during the recording. Electron diffraction patterns were obtained on a JEOL 200CX apparatus.

Results and Discussion

Electrochemical alkali metal insertion into $NbTe_2$ was performed by step potential electrochemical spectroscopy of lithium and sodium cells using $NbTe_2$ as cathodic material. This method has recently proven of particular interest in the study of the electrochemical behavior of γ-MnO_2[22] and C_{60}.[23] Up to 1.3 lithium atoms per formula unit was incorporated into the interlayer space of $NbTe_2$. The total number of distorted octahedral sites defined by consecutive $NbTe_2$ slabs (2d and 4i sits of $C2/m$ space group) allow a maximum composition of $LiNbTe_2$. For larger contents, the possible occupancy of distorted tetrahedral sites may be assumed. However, this site occupancy is not favored as evidenced by a steep decrease in incremental capacity for $x >$ 1.2. Incremental capacity vs composition curves of the lithium cell (Figure 2a) reveal an asymmetric and broad reduction band indicative of the progressive filling of the available intercalation sites. No low-intensity peaks similar to those ascribed to lithium ordering for TiS_2[19] or VTe_2[20] were present, although the asymmetry of the reduction peak may be indicative of this phenomenon with energetically similar intermediate situations. A slow relaxation of the current was observed during the reduction effect indicative of a slow diffusion of lithium ions in a wide composition interval. The complex changes in slope found in the I vs x plots (Figure 2b) in the 0.6–0.8 interval could be indicative of the coexistence of phases with different lithium ordering in the interlayer space.

An incremental capacity peak at ca. 1.2 V, and a shoulder at 1.4 V are resolved in the step potential electrochemical spectra of the sodium cells (Figure 2c). At each potential within these effects, a slow current relaxation was observed, as expected by sodium ion diffusion during the two different steps of the intercalation process. From the plot in Figure 2d, it can be seen that the values of x at which the peaks corresponding to two-phase regions occur show little changes during current relaxation; i.e., the stoichiometry at which the reduction effects are developed has a negligible shift with scanning rates above ~10 mV/h. The composition limits for these successive electron plus ion injection processes are located at ca. $x = 0.6$ and $x = 1.0$ respectively.

The XPD patterns of lithium intercalated samples showed the coexistence of pristine $NbTe_2$ and lithiated product in the $0 <$

(22) Chabre, Y. *J. Electrochem. Soc.* **1991**, *138*, 329.
(23) Chabre, Y.; Djurado, D.; Armand, M.; Romanow, W. R.; Coustel, N.; McCauley, J. P.; Fischer, J. E.; Smith, A. B. *J. Am. Chem. Soc.* **1992**, *114*, 764.

Table 1. Powder X-ray Diffraction Data for $LiNbTe_2$

h k l	d_{obs} (Å)	d_{calc} (Å)	I/I_o	h k l	d_{obs} (Å)	d_{calc} (Å)	I/I_o
0 0 1	7.219	7.215	100	−8 0 4	2.268	2.269	16
0 0 2	3.611	3.607	50	−10 0 4	1.933	1.930	15
−6 0 3	3.026	3.025	28	0 0 4	1.814	1.804	23
3 1 0	2.925	2.927	63	−6 2 2	1.621	1.625	8
−5 1 3	2.458	2.462	15	−11 1 6	1.456	1.455	6
0 0 3	2.401	2.405	25	−8 2 6	1.249	1.249	8

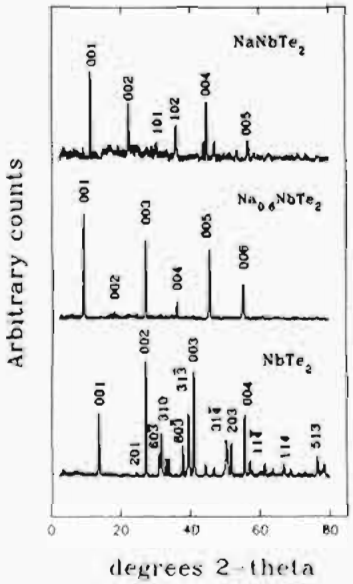

Figure 3. XPD patterns of pristine $NbTe_2$ and sodium intercalated products.

$x < 1$ interval. For $x = 1$, the XPD patterns were characteristic of a single-phase product (Table 1). The pattern is still indexable in the $C2/m$ space group, as a result of the topotactic nature of the process. An increase in the pseudohexagonal c_h parameter normal to the layers ($c_m \sin \beta_m$) of ca. 0.5 Å was observed. Similar results were obtained by Murphy et al.[9] by chemical intercalation of lithium into $NbTe_2$. XPD data also show that c_m and the unit cell volume are significantly larger in $LiNbTe_2$ ($a_m = 19.45_1$ Å, $b_m = 3.751_5$ Å, $c_m = 10.00_1$ Å, $\beta_m = 133.91_5°$, $V = 526$ Å^3) than in $NbTe_2$ ($a_m = 19.24_1$ Å, $b_m = 3.630_2$ Å, $c_m = 9.269_4$ Å, $\beta_m = 134.47_2°$, $V = 462$ Å^3). Less pronounced changes in a_m, b_m, and β_m may be a consequence of lattice adaptation to the changes in electron count due to partial electron donation from incoming lithium atoms.

The XPD patterns of sodium intercalated products differ significantly. For $Na_{0.6}NbTe_2$ and $NaNbTe_2$, single phase products were detected (Figure 3), in agreement with the composition limits of stability shown by step potential electrochemical spectroscopy. XPD data of intermediate compositions showed the coexistence of $NbTe_2$ and $Na_{0.6}NbTe_2$ for $0.6 > x > 0$ and of $Na_{0.6}NbTe_2$ and $NaNbTe_2$ for $1 > x > 0.6$. Preferred orientation phenomena condition (00l) lines to have an enhanced intensity and do not allow a complete structural refinement. Nevertheless, the pattern for $NaNbTe_2$ was indexable in the hexagonal system ($a = 3.641_1$ Å, $c = 8.01_2$ Å) and the interlayer expansion Δc_h takes a value of 1.4 Å. The observed interlayer expansion is consistent with trigonal prismatic coordination of Na ions. A simplified analysis of the (00l) intensities[24] agrees with a model based in the complete occupancy of each interlayer space by Na ions, by using a –Na–Te–Nb–Te–stacking sequence. For $Na_{0.6}NbTe_2$, multiple order reflections of the basal spacing agree with a largely expanded cell with c_h of 9.89 Å. This effect may be indicative of the occurrence of Na-ordered phases as the different stages found for Na-intercalated TiS_2.[19] However, a model based in stage II or stage III phases could not describe accurately the observed intensities and spacings. Electron diffraction data give additional evidence about the structure of these products.

(24) Yvon, K.; Jeitschko, W.; Parthe, E. Lazy Pulverix, a programme to calculate theoretical X-ray and neutron diffraction powder patterns. Universite de Geneve, Switzerland, 1977.

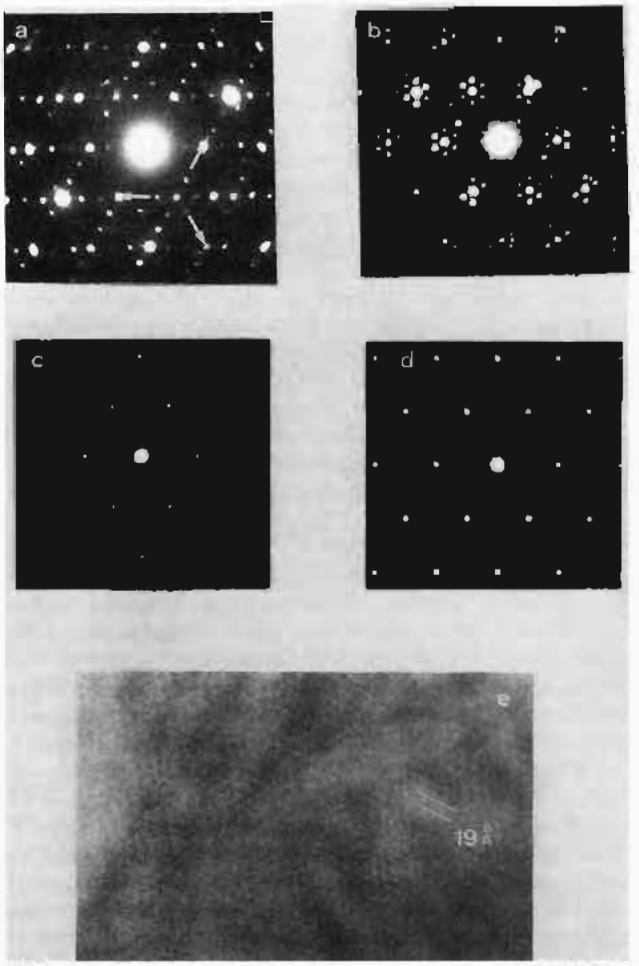

Figure 4. (a–d) {001} zone electron diffraction patterns of (a) 1T-$NbTe_2$, (b) $Na_{0.6}NbTe_2$, (c) $Na_{0.8}NbTe_2$ and (d) $NaNbTe_2$. (e) Bright field real space lattice image of 19 × 19 Å^2 modulations in $Na_{0.6}NbTe_2$.

Electron diffraction patterns of monoclinic 1T-$NbTe_2$ recorded with the electron beam lying almost parallel to [001] (Figure 4a) consist of alternate rows of $hk0$ spots that fulfil the $h + k = 2n$ condition of the $C2/m$ space group, in agreement with the crystallographic description of Brown[16] and the unit cell parameters obtained from XPD measurements. The in-plane $3a3^{1/2} \times a$ superstructure is evidenced by comparison with the undistorted [001] zone electron diffraction pattern of hexagonal 1T-MX_2. The superstructure results from the presence of ribbon chains that run along [100]. Additional complexity of the pattern results from three sets of rows differing by 60° (Figure 4a) suggesting that the particles consist of domains with three relative orientations. A similar description was reported for 1T-VTe_2[17] and its alkali metal intercalated products.[20] Such pattern is also observed in very thin lamellae, which may be indicative that particularly small domains are present or that the three orientations coexist in the same crystallite. Systematic absences prevent the positive identification of a possible $3a3^{1/2} \times 3a3^{1/2}$ superstructure in the solid.

The multidomain character of the particles is preserved during lithium intercalation and the pattern obtained for $LiNbTe_2$ is equivalent to that shown in Figure 4a. The fact that the ribbon chain modulation remains basically unaltered is probably a consequence of a partial covalent character of Li–Te bonding. On the contrary, the electron diffraction data of $NaNbTe_2$ reveal an undistorted hexagonal pattern (Figure 4d), similar to that

found at room temperature in some d^2 phases, as α-$MoTe_2$, which evidences the loss of the ribon chain modulation.

The electron diffraction patterns of $Na_{0.6}NbTe_2$ particles (Figure 4b) recorded at room temperature show further complexity. New extra spots occur that can be descriged by a $a27^{1/2} \times a27^{1/2}$ cell without any systematic absence. This is one of the allowed modulations with hexagonal symmetry in which the superstructure unit cell vectors $a_s = ma + nb$ and $b_s = -ma + (m + n)b$ with $n = m = 3$ define a cell which contains $m^2 + n^2 + mn = 27$ metal atoms in each layer.[25] This superstructure differs from those previously found in 1T-transition metal dichalcogenides. These are normally found in the *m,n* series with $n = 0$ (2,0 or $2a \times 2a$, 3,0 or $3a \times 3a$), $n = 1$ (1,1 or $a3^{1/2} \times a3^{1/2}$, 2,1 or $a7^{1/2} \times a7^{1/2}$, 3,1 or $a13^{1/2} \times a13^{1/2}$) and $n = 2$ (3,2 or $a19^{1/2} \times a19^{1/2}$). In these series, the number of metal atoms included in the supercell form either regular polygons or a combination of regular polygons and isolated atoms when $n = 0$. For $m = n > 1$ the resulting superstructures are multiple of the $a3^{1/2} \times a3^{1/2}$ modulation.

On the other hand, the $a27^{1/2} \times a27^{1/2}$ cell cannot be described as simple superposition of domains with $3a3^{1/2} \times a$ superlattice. Nevertheless its origin may be related to the presence of the three orientations of Nb ribbons in the crystals of pristine $NbTe_2$. The trimerization of a single layer of ribbons which is schematically shown in Figure 1c leads to a $3a \times 3a$ superlattice. In $NbTe_2$ however, the ribbons of consecutive slabs are not superimposed. In fact, the unit cell of isostructural VTe_2 was first described as triclinic with $a_t = 3a_h$ and $b_t = a_h$. The trimerization of this cell leads to the $3a \times 3a$ modulation as shown in Figure 1c. The true $3a3^{1/2}$ - *a* superlattice found in VTe_2 and $NbTe_2$ leads to a $a27^{1/2} \times a27^{1/2}$ superlattice as a result of the distribution of ribbons in consecutive layers. Moreover, if trigonal prismatic coordination of Na ions is assumed as in $NaNbTe_2$, the minimum displacements required between consecutive slabs, for example by $[100]_m/6$, make necessary to use a $3a3^{1/2} \times 3a3^{1/2}$ cell to describe the complete structure. Real space imaging of these particles show the occurrence of 19 × 19 Å^2 hexagonal domains, in agreement with the expected metal distribution in the superlattice. This model may explain the enhanced (*00l*) line intensity in the XPD pattern for $l = 2n + 1$, as $c_h \simeq 2a$.

When sodium content is increased, long modulations with hexagonal symmetry and values close to $3a3^{1/2} \times 3a3^{1/2}$ (Figure 4b), $4a3^{1/2} \times 4a3^{1/2}$ (Figure 4c) and $5a3^{1/2} \times 5a3^{1/2}$ occur, which may be ascribed to progressive filling of the d-block band by electron donation from sodium in the composition interval $Na_{0.6-1.0}NbTe_2$.

The relationship between electron count and the adoption of these structural modifications must take into account two different effects. First the interlayer Te–Te distances are notably increased by sodium intercalation. As a consequence, p-block to d-block electron donation within each slab is inhibited. On the other hand, upon intercalation of 0.6 Na ion per formula unit, 0.6 electron is added to the *d* block band. The final count is close to $d^{5/3}$, which differs from the initial $d^{4/3}$ and may be the origin of the trimerization. It is noteworthy the close relationships between this system and Na_xTaS_2.[14] For $NaNbTe_2$, the large interlayer expansion due to sodium insertion in trigonal prismatic coordination inhibits interlayer Te–Te interactions, thus decreasing d-electron count to 1. Simultaneously, electron donation from the incoming sodium increase d-band filling up to an electron count close to d^2, and consequently the modulations are inhibited.

The absence of such structural distortion in Li-intercalated products is consistent with the larger covalent character of the lithium–chalcogenide bonds as compared with sodium–chalcogenide bonds that inhibits an extended electron donation to the transition metal bands. On the other hand, the absence of such distortions in Na_xVTe_2[20] is consistent with the lower interlayer expansion found in that system that agrees with octahedral site occupancy of the Na ions.

Acknowledgment. We express our gratitude toward the CICYT (Contract PB92-0755-MOD.C) for the financial support of this work and to Consejería de Educación y Ciencia de la Junta de Andalucía.

(25) van Landuyt, J.; Wiegers, G. A.; Amelinckx, S. *Phys. Status. Solidi A* 1978, *46*, 479.